# DEVELOPMENT OF A METHOD FOR EXTRACTING DISASTER AREAS AROUND INFRASTRUCTURES USING MULTI-TEMPORAL SAR IMAGES

Tomoya Kusunose[1] and Junichi Susaki[1]
[1]Kyoto University, C1-1-206, Kyotodaigaku-katsura, Nishikyo-ku, Kyoto 615-8540, Japan,
Email: {kusunose.tomoya.37w@st., susaki.junichi.3r@}kyoto-u.ac.jp

**KEY WORDS:** Synthetic Aperture Radar (SAR), PSI, heavy rainfall disaster, detection of disaster areas

**ABSTRACT:** In recent years, torrential rains caused by global warming have become more serious and frequent, causing extensive damage to various infrastructures. In order to reduce the damage, preventive maintenance is desirable. In contrast, surveying localized ground surface changes by hand is difficult. Therefore, effective and efficient implementation of national land monitoring is required. Nowadays, the use of Synthetic Aperture Radar (SAR) imagery is expected to provide a comprehensive view of the earth's surface, independent of weather conditions and time of day. Differential interferometric SAR (DInSAR) technique has been widely known as wide range of land subsidence measurement method. In particular, Persistent Scatterers Interferometry (PSI) can accurately measure wide range of land subsidence by using multi-temporal SAR images. Based on the accurately estimated ground displacement velocity, we can detect small ground displacement behavior before a disaster occurs, which may be useful for disaster management. In this paper, PSInSAR analysis was conducted around the Takeo Junction (JCT) in western Japan, where a large landslide occurred in the past due to a heavy rainfall disaster and the road surface was uplifted significantly. After that, we conducted a basic study on the development of a method for detecting signs of disaster based on ground displacement velocity. As a result, we can detect the behavior of the ground pushing up the road surface before a landslide occurs. This result suggests the possibility of using satellite SAR imagery to detect signs of a disaster.

## 1. INTRODUCTION

A landslide occurred at the Takeo JCT, located in western Japan, due to a torrential rain disaster in August 2019. The road surface uplift occurred due to the slope displacement of the expressway, and it took about a year to restore the road. In the past few years, torrential rains have become more serious and frequent in Japan, causing extensive damage to various infrastructures. In order to reduce the damage, preventive maintenance should be carried out not only to quickly determine the extent and scale of damage, but also to predict the occurrence of damage in advance. In contrast, surveying all local changes in the ground surface by hand is very costly. Furthermore, in some cases, it is difficult for people to enter forest areas. Therefore, for effective and efficient national land monitoring, the use of Synthetic Aperture Radar (SAR) imagery is expected to enable us to grasp the surface of the earth at once.

As a general method for extracting disaster areas, coherence analysis is used (Karamura et al., 2011 and Plank, 2014). In coherence analysis, several SAR images are interfered with each other across the time of the disaster. Then, thresholding is performed based on the degree of interference (coherence). Finally, the area with the lower coherence value is extracted as the disaster areas. However, this method uses only a few images and is prone to error components such as noise. Therefore, the disaster areas may not be extracted as a significant variation. Coherence analysis has low sensitivity to small displacement and cannot detect small ground displacement behavior. Furthermore, the coherence value itself has no meaning. This makes the setting of the threshold intentionally, and the lack of versatility of the coherence analysis is a problem.

As an interpretable geophysical quantity, the ground displacement velocity can be used. Differential Interferometric SAR (D-InSAR) is widely known as a method to estimate the velocity of ground displacement using SAR images. It is a method to estimate the displacement based on the difference of the microwave phase of the two time images. In recent years, more accurate time series SAR analysis is used. This method extends the dimension of D-InSAR in the time direction, which enables highly accurate estimation. In particular, PSInSAR (Ferretti et al., 2001) extracts pixels containing permanent scatterers (PS) from multi-temporal SAR images and performs D-InSAR. This statistically reduces the influence of noise and allows for highly accurate estimation of the ground displacement velocity. PSInSAR is used in a number of studies to monitor the displacement of infrastructures (Sousa and Bastos, 2013) and land subsidence (Yu et al., 2009 and Jiang et al., 2021). However, no research has attempted to apply the estimated displacement velocity to disaster management.

In this paper, we will estimate the ground displacement velocity using PSInSAR around the Takeo Junction (JCT) located in western Japan. The study area suffered from a large landslide caused by a heavy rainfall disaster in the past,

and the surface of the highway was raised significantly. Then, based on the estimated ground displacement velocity, a basic study for the development of a method to detect the signs of disaster will be conducted.

This paper is organized as follows. In Section 2 is the method to estimate the ground displacement velocity in Takeo JCT. The study area and data used is described in Section 3. The results are shown in Section 4. In Section 5, the validity of the estimated results is discussed. Finally, this paper is concluded in Section 6.

## 2. METHOD

In this section, we describe a method of estimating the ground displacement velocity using PSInSAR, a type of time series SAR analysis. In PSInSAR, pixels that contain permanent scatters (PS) are extracted and D-InSAR is performed on them. PS is the pixel for which the effect of noise is statistically determined to be small using multiple SAR images. This technique reduces the error that is problem with D-InSAR, and allows us to obtain the velocity of variation in mm unit. we will conduct the analysis with PSInSAR. The flow of the PSInSAR analysis in this paper is shown in Figure 1 (Ferretti et al., 2001). When creating a differential interferogram, PSInSAR selects one SAR image as the master image from N+1 SAR images, and creates N differential interferograms with the other images as slave images. For the selection of the master image, the master image is chosen so that it has good coherence with the other slave images. In general, the interferometric worsens as the time and vertical baseline lengths increase. Therefore, the master image is selected to minimize the temporal and vertical baseline lengths. In addition, a smoothing filter was applied during the analysis to increase the number of analysis points and improve the accuracy. The size of the filter was set to 100 pixel × 100 pixel (about 300 m × 300 m).

Normally, the estimation of the displacement velocity in PSInSAR is based on the approximation of the cumulative displacement to calculate the average rate of change. However, this approach makes it difficult to ascertain at what point in the time axis there were signs of a disaster. In this paper, we calculate the velocity of the image data every two time periods from the cumulative displacement obtained by PSInSAR (shown in Figure 2(b)).

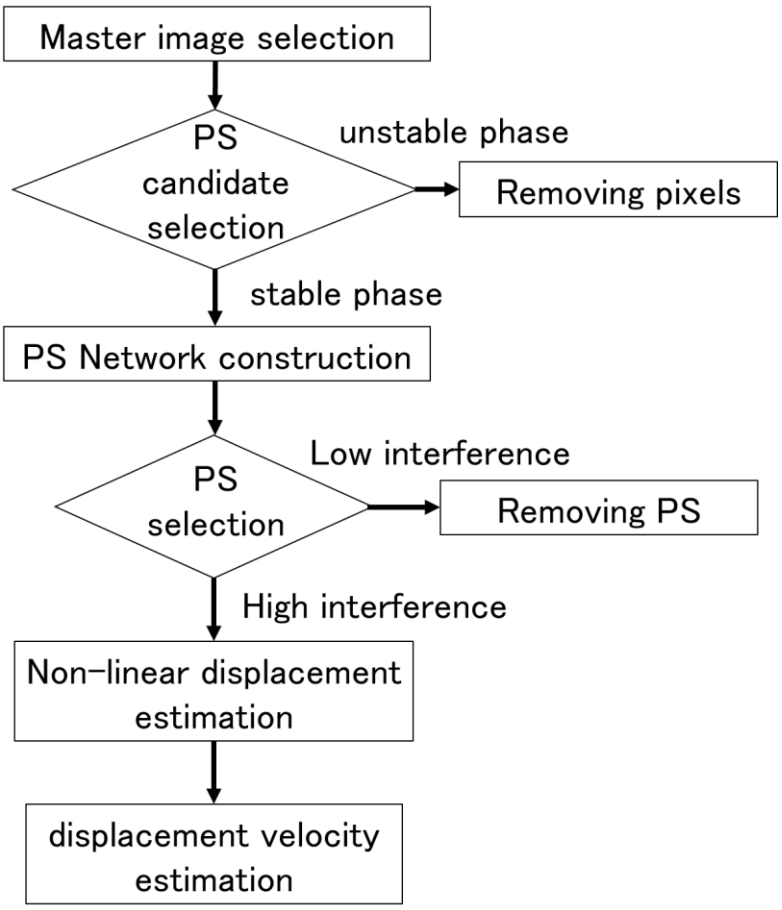


Figure 1. Flowchart of PSInSAR

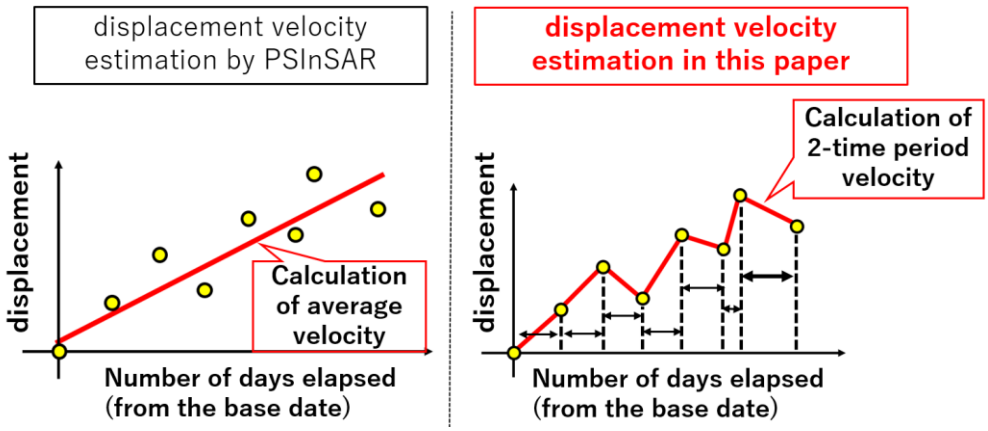


(a) (b)

Figure 2. Estimation of the velocity of PSInSAR. (a) displacement velocity estimation by PSInSAR. (b) displacement velocity estimation in this paper.

## 3. STUDY AREA AND DATA USED

In this study, the Takeo JCT (shown in Figure 3), located in western Japan, was chosen as the analysis area. The area around the Takeo JCT suffered from disasters caused by heavy rain every year from 2017 to 2020. Specifically, they are July 5 to July 6, 2017, June 5 to July 8, 2018, August 27 to August 29, 2019, and July 3 to July 31, 2020 (shown in Table 1). In particular, the torrential rain disaster that occurred in 2019 caused slope displacement of the road surface at the Takeo JCT, resulting in road surface abnormalities. The disaster was caused by a rapid rise in groundwater levels and a decline in ground strength due to abnormal rainfall. The area in the red frame in Figure 1 is the area around the landslide (West Nippon Expressway Company Limited.).

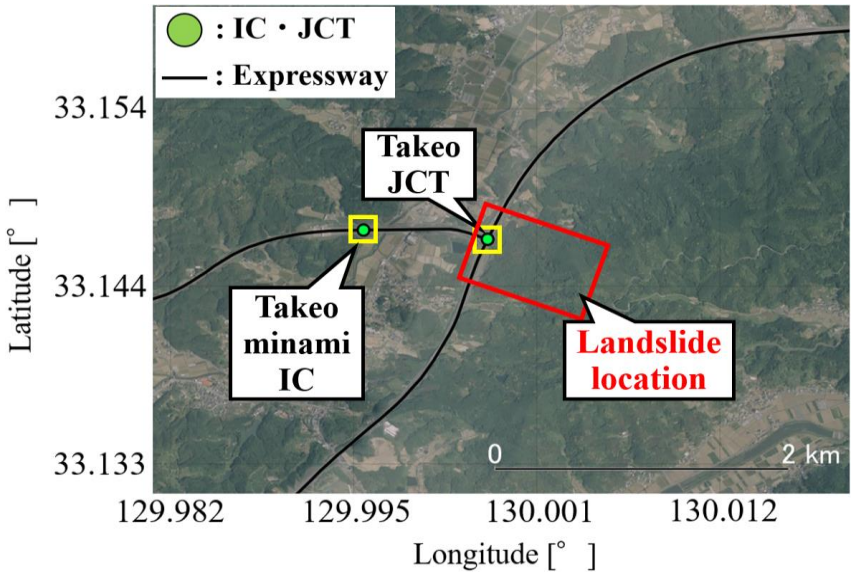


Figure 3. Overview of Takeo JCT from nadir view (Geographical Survey Institute). Green dots indicate nodes (IC and JCT). The black line indicates an expressway.

Table 1. History of disasters in the area around Takeo JCT (Kyushu Disaster History Information Database)

| Date | Types of Disasters | Forms of damage |
|---|---|---|
| 2017/07/05 – 07/06 | Torrential rain | Flooding |
| 2018/07/05 – 07/08 | Torrential rain and typhoons | Flooding |
| 2019/08/27 – 08/29 | Torrential rain | Landslide disaster and Flooding |
| 2020/07/03 – 07/31 | Torrential rain | Flooding |

We used 15 descending-orbit SAR images taken by PALSAR 2 onboard ALOS 2 from February 2017 to October 2020, in which the observation mode was Ultra-fine-Beam mode Single polarization (UBS) and the observation direction was all to the right. Table 1 summarizes the shooting time, observation mode, and baseline length. The spatial and temporal baseline lengths are relative to the master image. We used the 90 m grid SRTMDEM to remove the effect of topography.

Table 2. Used SAR images. Perp. Baseline and Temp. baseline are relative values with respect to the master image.

| No. | Date | Perp. Baseline [m] | Temp. baseline [days] |
|---|---|---|---|
| 1 | 2017/02/25 | 175 | -616 |
| 2 | 2017/06/03 | 25 | -518 |
| 3 | 2017/08/12 | 66 | -448 |
| 4 | 2017/11/04 | -162 | -364 |
| 5 | 2018/02/24 | 291 | -252 |
| 6 | 2018/06/02 | 220 | -154 |
| 7 | 2018/08/11 | 130 | -84 |
| 8 | 2018/11/03 | Master image | |
| 9 | 2019/02/23 | 1314 | 112 |
| 10 | 2019/08/10 | -16 | 280 |
| 11 | 2019/11/02 | -21 | 364 |
| 12 | 2020/02/22 | -244 | 476 |
| 13 | 2020/05/30 | 126 | 574 |
| 14 | 2020/08/08 | -13 | 644 |
| 15 | 2020/10/31 | -70 | 728 |

## 4. RESULT

Figure 4. shows the result of the estimated displacement velocity of the image data based on PSInSAR for each two periods. In addition, the inside of the red frame in the Figure 4. shows the area around the actual landslide area. In the two periods between the occurrence of heavy rainfall (“2017-06-03 – 2017-08-12”, “2018-06-02 – 2018-08-11”, “2019-08-10 – 2019-11-02” and “2020-05-30 – 2020-08-08”), the right side of the red frame showed a tendency of increasing the rate of ground subsidence (shown in Figure 4 (b), (f), (j), (m)). In the results of “2018-11-03 - 2019-02-23”, the subsidence rate increased in the right side region in the red frame and the uplift rate increased towards the left side. The ground displacement that pushed up the road surface was confirmed (shown in Figure 4 (h)). Furthermore, a clear tendency to push up the road side was detected in the analysis results for “2020-08-08 - 2020-10-31” (shown in Figure 4 (n)).

In contrast, although landslide and road surface uplift phenomena actually occurred during the 2019 torrential rains, the results of the analysis after the 2019 torrential rains period (“2019-08-10 – 2019-11-02”) showed that the overall rate of change was not very large (shown in Figure 4 (j)).

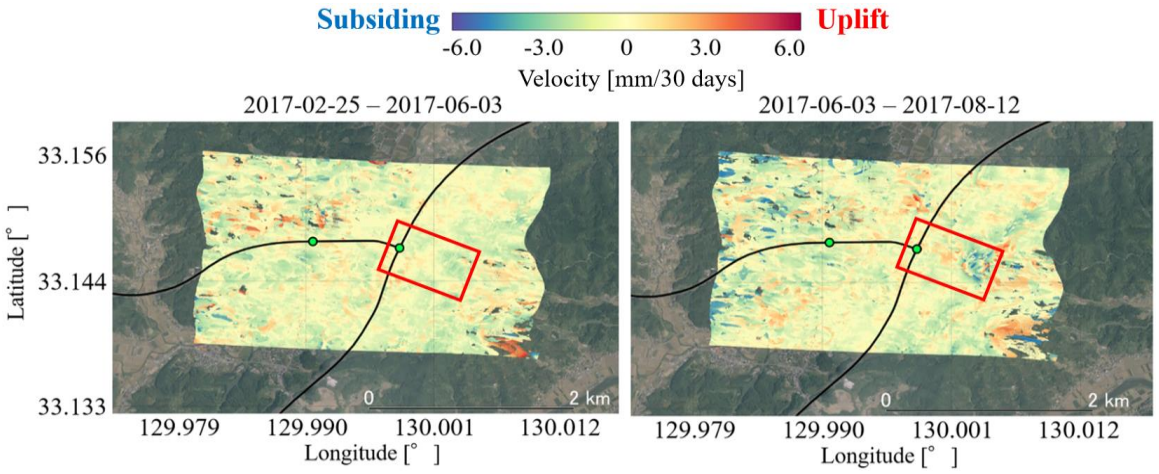

(a) (b)

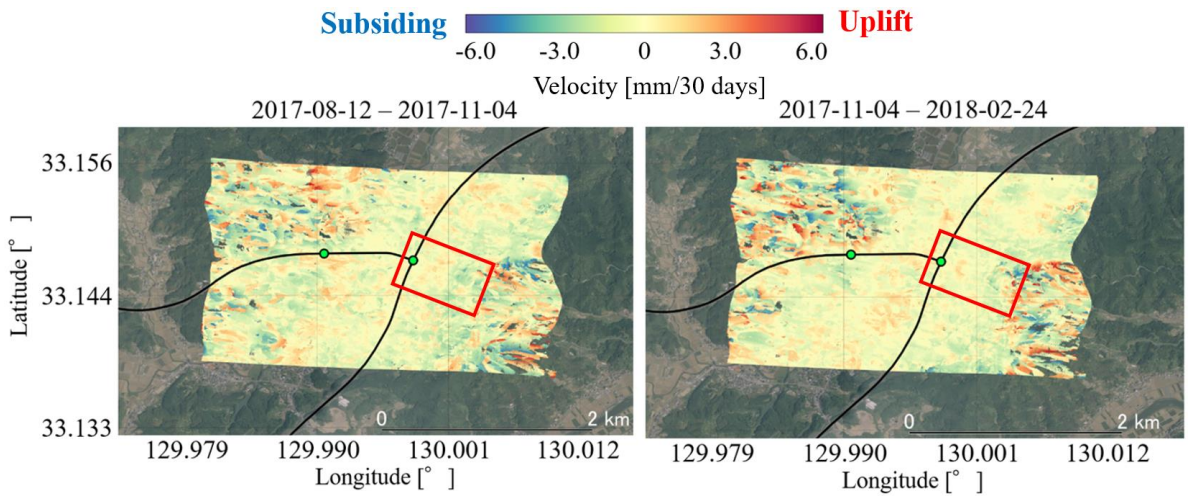
Subsiding
Uplift
-6.0 -3.0 0 3.0 6.0
Velocity [mm/30 days]
2017-08-12 – 2017-11-04
2017-11-04 – 2018-02-24
33.156
33.144
33.133
Latitude [° ]
0
2 km
129.979 129.990 130.001 130.012
Longitude [° ]

(c) (d)

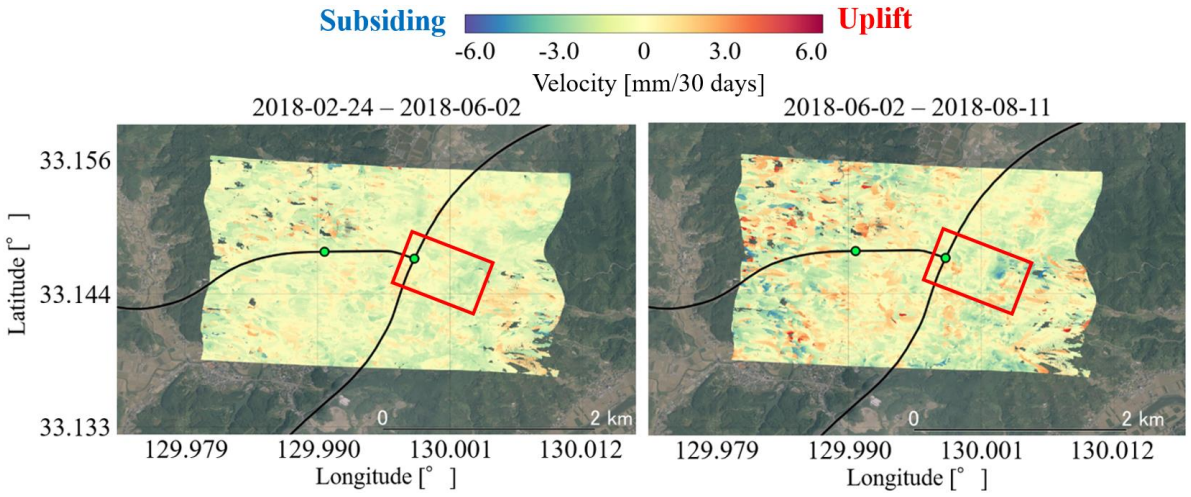
Subsiding
Uplift
-6.0 -3.0 0 3.0 6.0
Velocity [mm/30 days]
2018-02-24 – 2018-06-02
2018-06-02 – 2018-08-11
33.156
33.144
33.133
Latitude [° ]
0
2 km
129.979 129.990 130.001 130.012
Longitude [° ]

(e) (f)

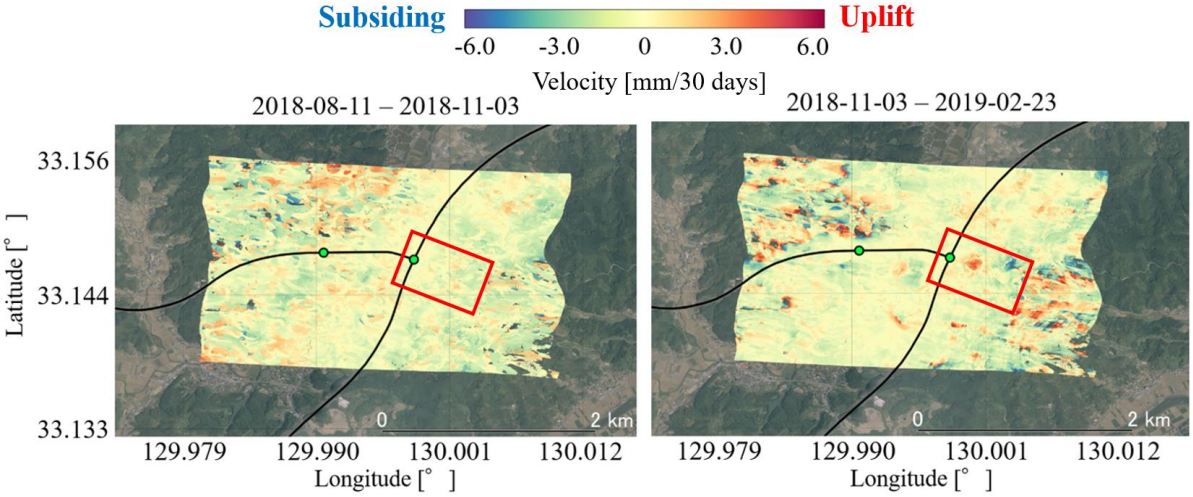
Subsiding
Uplift
-6.0 -3.0 0 3.0 6.0
Velocity [mm/30 days]
2018-08-11 – 2018-11-03
2018-11-03 – 2019-02-23
33.156
33.144
33.133
Latitude [° ]
0
2 km
129.979 129.990 130.001 130.012
Longitude [° ]

(g) (h)

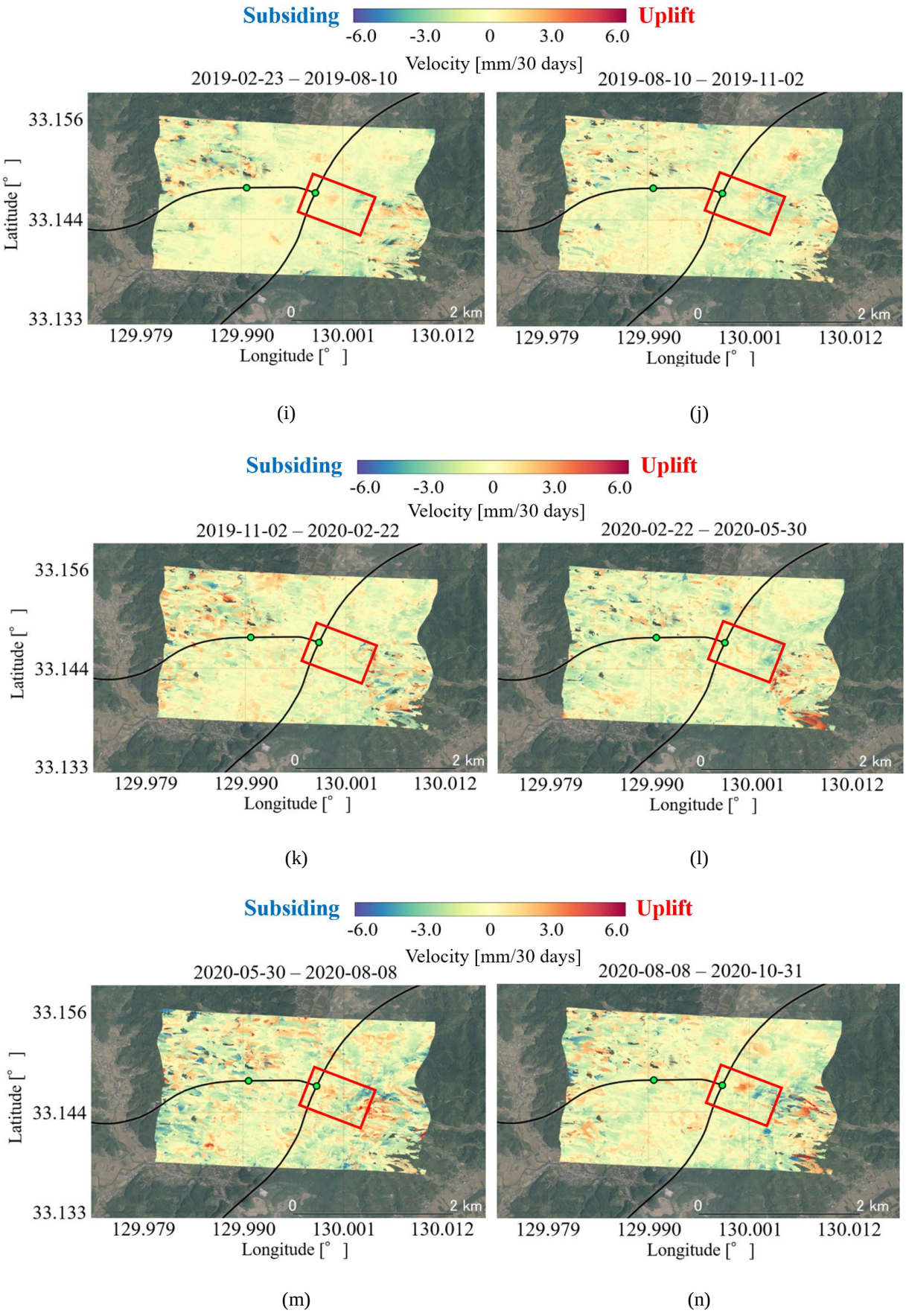


Figure 4. Estimated displacement velocity distribution for each of the two periods calculated based on the cumulative displacement of PSInSAR. (a) – (n) Estimated displacement velocity in each of the two periods.

We focus on areas other than the red frame. The upper left and lower right areas of the analysis area show a complicated distribution of displacement velocity, especially, "2017-11-04 – 2018-02-24" and "2018-11-03 – 2019-02-23" (shown in Figure 4 (d), (h)).

## 5. DISCUSSION

First, a discussion is made based on the topography around the Takeo JCT. In order to visualize the topographic data, we used the DEM data (5 m mesh) (Geographical Survey Institute) to calculate the slope angle, and slope azimuth angle of the terrain (Figure 5.).

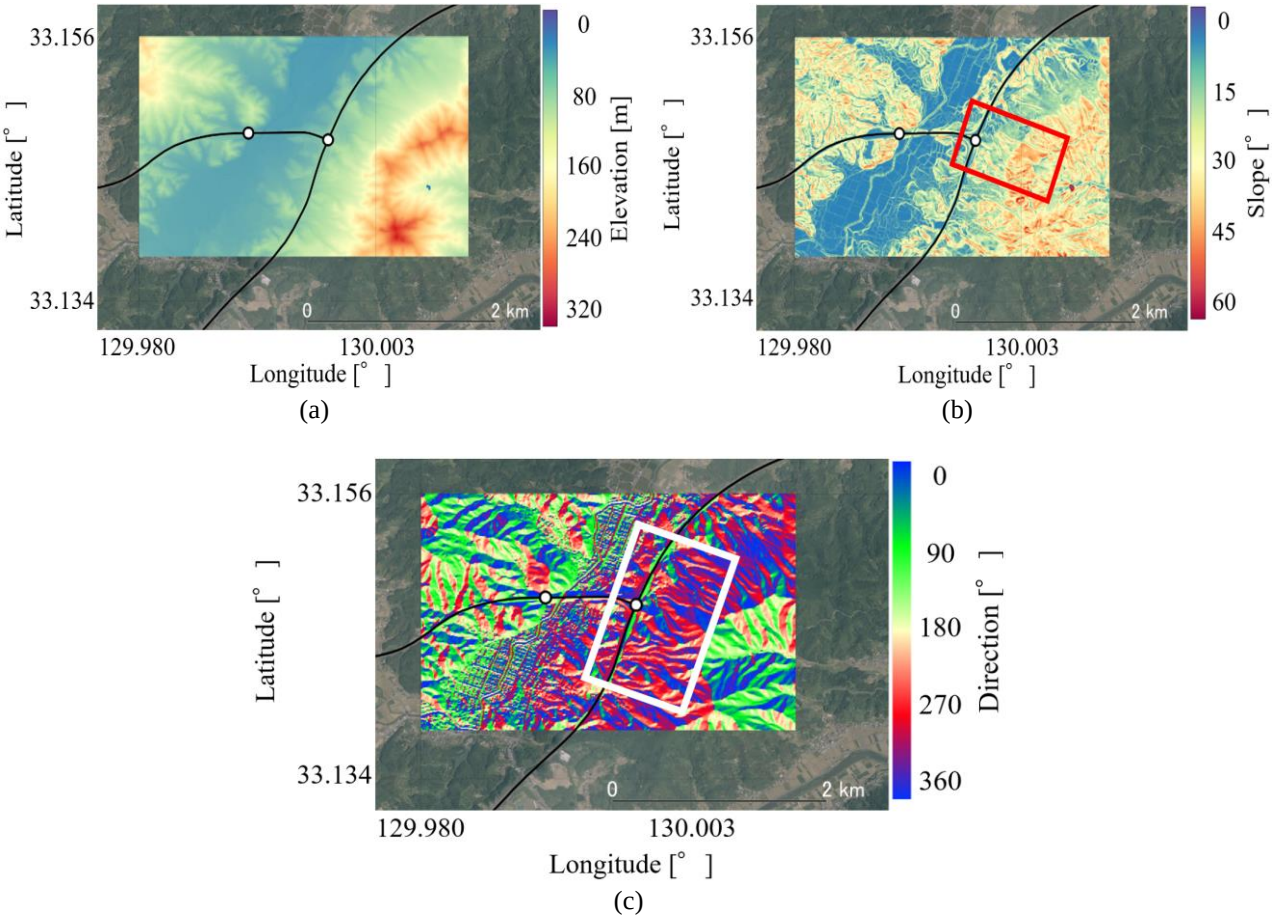


Figure 5. Topographic around Takeo JCT. Slope angle and slope azimuth angle are calculated from elevation. (a) elevation map, (b) slope map, (c) slope azimuth angle map.

From the results, the slope angle was large near the east side of the Takeo JCT where the landslide occurred, and the slope direction was toward the expressway (shown in Figure 5 (b),(c)). Therefore, the ground displacement behavior that pushes up the road surface obtained by PSInSAR is reasonable from the topographical conditions.

Next, we discuss the results of the ground displacement behavior that pushes up the road surface. The velocity distribution between each heavy rainfall event period from 2017 to 2020 shows that the rate of land subsidence tends to increase (shown in the black frame on the right of Figure 6 (a), (b), (d), (e)). In contrast, at this time, no uplift of the ground is observed yet (shown in the red frame on the left of Figure 6 (a), (b), (d), (e)). The trend of ground displacement behavior that clearly pushes up the road surface was observed in the period "2018-11-03 - 2019-02-23" and "2020-08-08 - 2020-10-31", after some time passed from the heavy rain disaster (shown in Figure 6 (c), (f)). The results suggest that the ground is softened by the torrential rain disaster and the soil pressure was continuously applied against the road. In particular, the results of "2018-11-03 - 2019-02-23" pushing out the road surface occurred before the landslide caused by the 2019 heavy rains. Therefore, this phenomenon may have been detected as a sign of the occurrence of landslide and road uplift disasters.

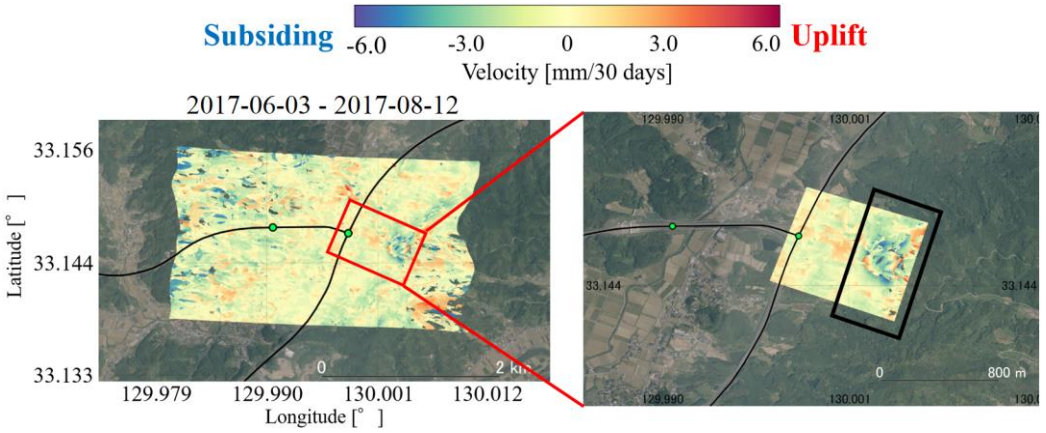
Subsiding
-6.0
-3.0
0
3.0
6.0
Uplift
Velocity [mm/30 days]
2017-06-03 - 2017-08-12
33.156
33.144
33.133
Latitude [° ]
129.979
129.990
130.001
130.012
Longitude [° ]
0
2 km
129.990
130.001
33.144
0
800 m

(a)

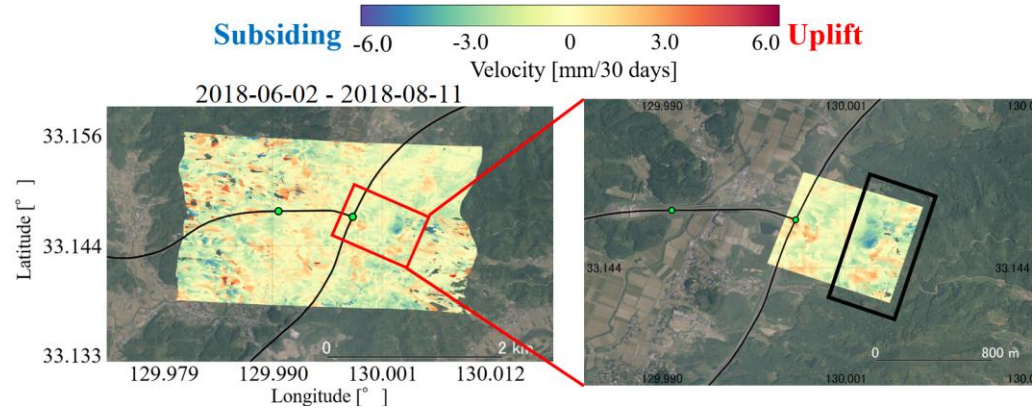
Subsiding
-6.0
-3.0
0
3.0
6.0
Uplift
Velocity [mm/30 days]
2018-06-02 - 2018-08-11
33.156
33.144
33.133
Latitude [° ]
129.979
129.990
130.001
130.012
Longitude [° ]
0
2 km
129.990
130.001
33.144
0
800 m

(b)

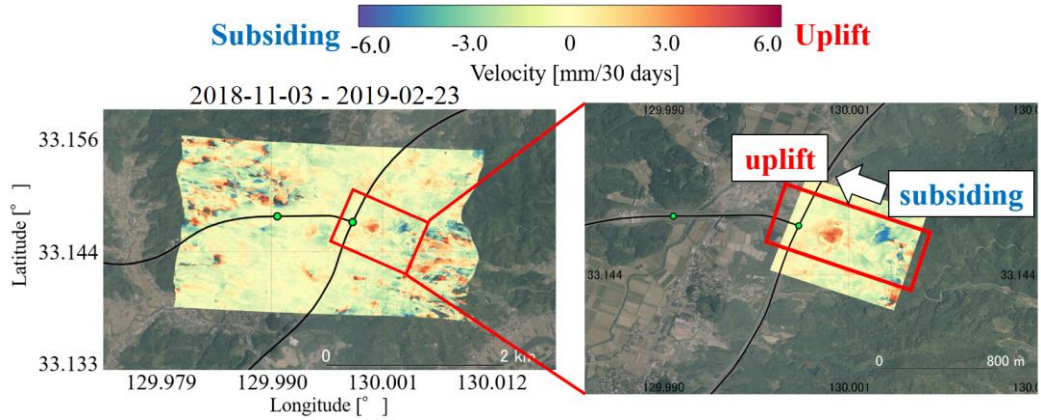
Subsiding
-6.0
-3.0
0
3.0
6.0
Uplift
Velocity [mm/30 days]
2018-11-03 - 2019-02-23
33.156
33.144
33.133
Latitude [° ]
129.979
129.990
130.001
130.012
Longitude [° ]
0
2 km
129.990
130.001
uplift
subsiding
33.144
0
800 m

(c)

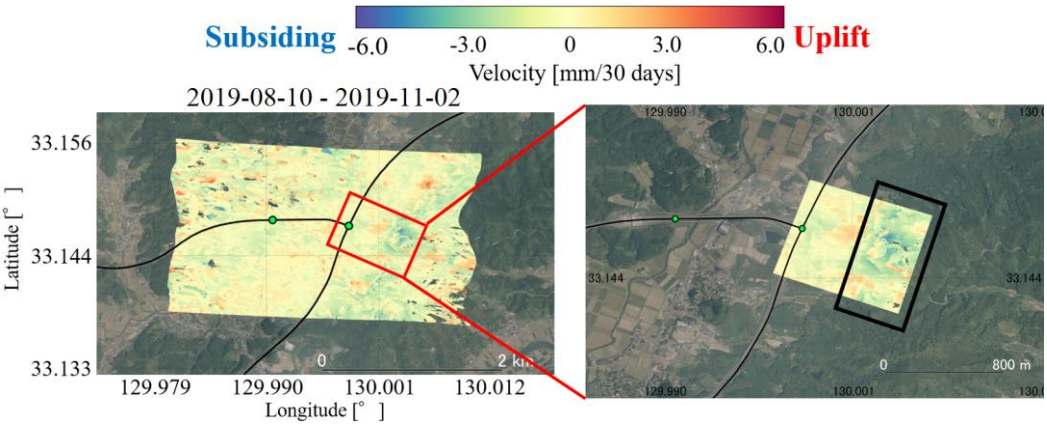
Subsiding
-6.0
-3.0
0
3.0
6.0
Uplift
Velocity [mm/30 days]
2019-08-10 - 2019-11-02
33.156
33.144
33.133
Latitude [° ]
129.979
129.990
130.001
130.012
Longitude [° ]
0
2 km
129.990
130.001
33.144
0
800 m

(d)

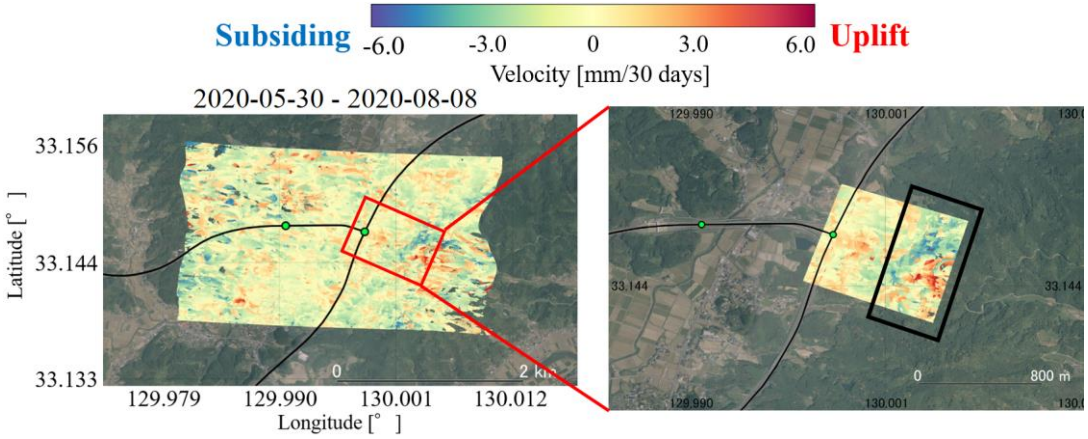


(e)

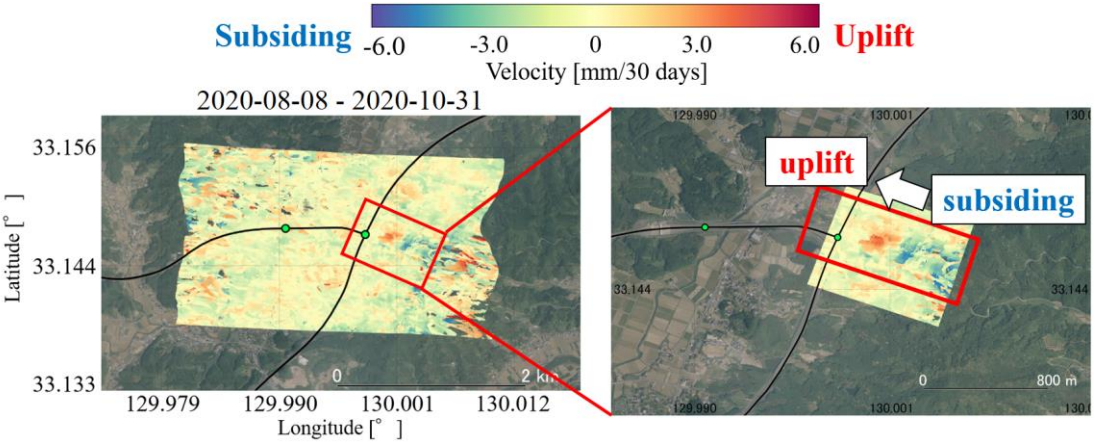


(f)

Figure 6. Enlarged view of landslide occurrence points in the distribution of ground displacement velocity in two periods. (a) the result of "2017-06-03 – 2017-08-12", (b) the result of "2018-06-02 – 2020-08-11", (c) the result of "2018-11-03 – 2019-02-23", (d) the result of "2019-08-10 – 2019-11-02", (e) the result of "2020-05-30 – 2020-08-08", (f) the result of "2020-08-08 – 2020-10-31".

Finally, we discuss the distribution of the disturbed displacement velocity in the upper left and lower right regions of the analyzed area in the results from "2017-11-04 - 2018-02-24" and "2018-11-03 - 2019-02-23" (shown in Figure 4 (d), (h)). In the white frame of Figure 7(a), the slope azimuth angles take a relatively complex distribution, indicating that the slope is directed in various directions. In addition, the black frames in Figure 7(b) and 7(c) correspond roughly to the position of the white frame in Figure 7(a). Therefore, due to the relatively complex slope direction, the ground may have shifted in all directions and the ground fluctuation rate may have been disorderly distributed.

## 6. CONCLUSION

In this study, we used PSInSAR to estimate the ground displacement velocity around the Takeo JCT, where landslides and ground uplift disasters occurred in the past. After that, based on the estimated velocity, we conducted a basic study on the development of a method for detecting signs of disaster occurrence. As a result of the analysis, ground displacement behavior that pushed up the road surface was confirmed before the landslide and road surface uplift disasters occurred. Therefore, the results suggest that satellite SAR images can be used to detect signs of disaster. In contrast, the analysis results "2019-08-10 - 2019-11-02" across the period of heavy rainfall in 2019, which triggered the landslide and road surface uplift disaster, showed that no significant rate of change occurred. Therefore, it is necessary to continue to study the extraction of disaster occurrence areas. As a future prospect, we will conduct a study on quantitative evaluation of ground displacement velocity and topographical data based on slope angle and slope azimuth angle. After that, we will assimilate the topographical data and rainfall data with the estimated ground displacement velocity. Then, we will start to develop a system for detecting the signs of landslide disasters.

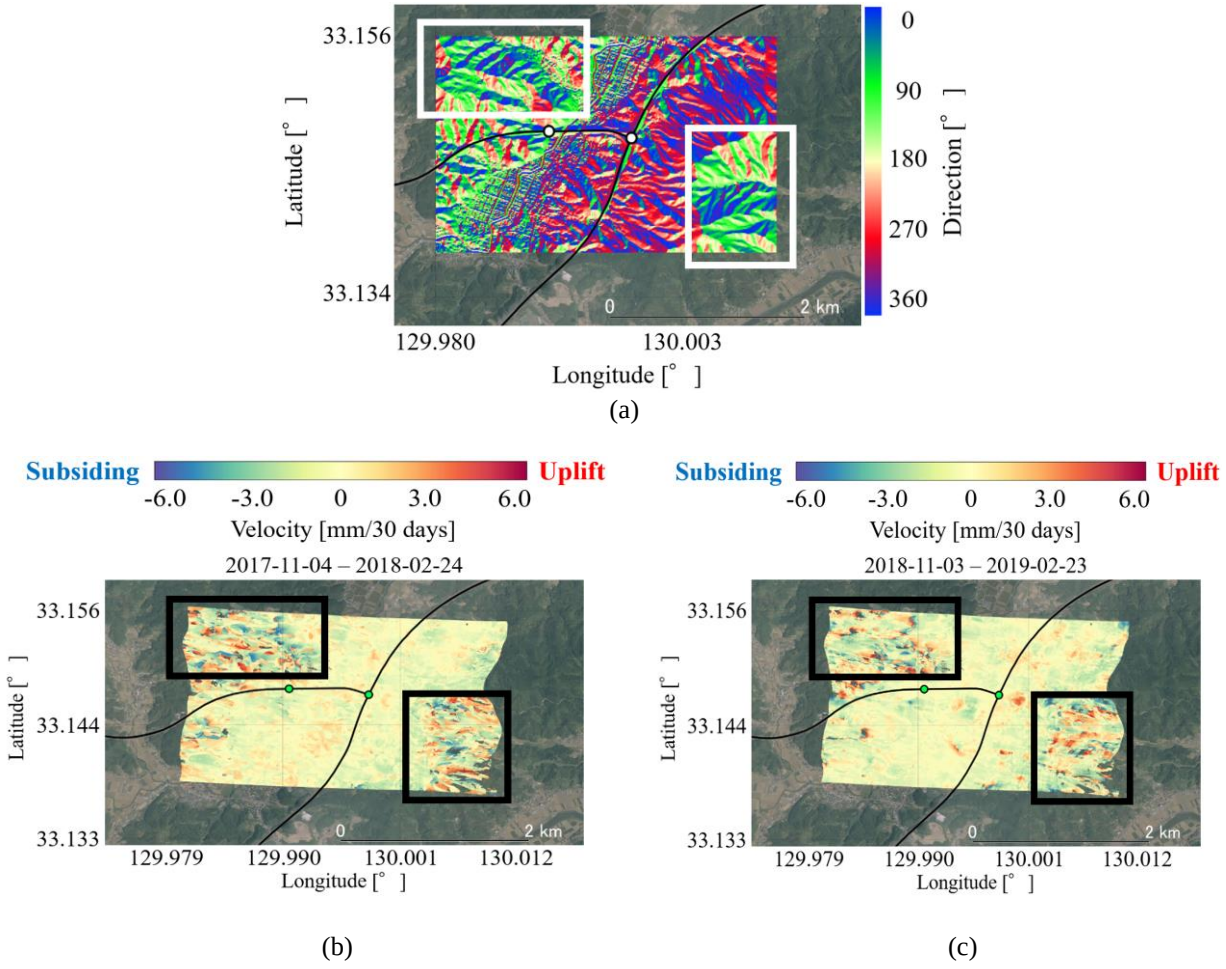


Figure 7. Comparison of slope azimuth angle distribution and displacement velocity distribution. (a) slope azimuth angle, (b) the result of estimated velocity "2017-11-04 - 2018-02-24", (c) the result of estimated velocity "2018-11-03 - 2019-02-23". The white frame in (a) shows a relatively complex distribution of slope azimuth angle, which corresponds to the disturbance of the displacement velocity in the black frames in (b) and (c).

**REFERENCES:**

Kawamura, J., Tsujino, K., Tsujiko, Y., and Tanjung, J., 2011. Detection method of slope failures due to the 2009 Sumatra earthquake by using TerraSAR-X images. 2011 IEEE International Geoscience and Remote Sensing Symposium, Symposium Proceedings, pp. 4292-4295.

Plank, S., 2014. Rapid Damage Assessment by Means of Multi-Temporal SAR – A Comprehensive Review and Outlook to Sentinel-1, Remote Sensing, vol. 6, pp. 4870-4906.

Sousa, J. J., and Bastos, L., 2013. Multi-temporal SAR interferometry reveals acceleration of bridge sinking before collapse, Natural Hazards and Earth System Sciences, 13(3), pp. 659-667

Yu, J., Ng, A., Jung, S., Ge, L., Rizos, C., 2009. Urban Monitoring using Persistent Scatterer InSAR and Photogrammetry, The International Archives of the Photogrammetry, Remote Sensing and Spatial Information Sciences. Vol. XXXVII. Part B1, pp. 257-262.

Jiang, H., Balz, T., Cigna, F., Tapete, D., 2021. Land Subsidence in Wuhan Revealed Using a Non-Linear PSInSAR Approach with Long Time Series of COSMO-SkyMed SAR Data, Remote Sensing, vol. 13(7), pp. 1256.

West Nippon Expressway Company Limited., Results of the 1st Technical Review Committee Meeting on Slope Disaster at Takeo JCT, Nagasaki Expressway, Retrieved September 12, 2021, from https://corp.w-nexco.co.jp/corporate/release/kyushu/r1/0903a/.

Geographical Survey Institute., Geographical Survey Institute Tile, Retrieved September 12, 2021, from https://maps.gsi.go.jp/development/ichiran.html.

Kyushu Disaster History Information Database., Saga prefecture, Retrieved September 12, 2021, from http://saigairireki.qscpua2.com/saga/.

Geographical Survey Institute., Fundamental Geospatial Data Download Service, Retrieved September 12, 2021, from https://fgd.gsi.go.jp/download/menu.php.